Editor's Choice



Quenching-Induced Defects Liberate the Latent Reversible Capacity of Lithium Titanate Anode

Zhong Su, Shunning Li, Lu Ma, Tongchao Liu, Meng Li, Tianpin Wu, Qinghua Zhang, Cheng Dong, Chao Lai, Lin Gu,* Jun Lu,* Feng Pan,* and Shanqing Zhang*

Interest in defect engineering for lithium-ion battery (LIB) materials is sparked by its ability to tailor electrical conductivity and introduce extra active sites for electrochemical reactions. However, harvesting excessive intrinsic defects in the bulk of the electrodes rather than near their surface remains a longstanding challenge. Here, a versatile strategy of quenching is demonstrated, which is exercised in lithium titanate (Li₄Ti₅O₁₂, LTO), a renowned anode for LIBs, to achieve off-stoichiometry in the interior region. In situ synchrotron analysis and atomic-resolution microscopy reveal the enriched oxygen vacancies and cation redistribution after ice-water quenching, which can facilitate the native unextractable Li ions to participate in reversible cycling. The fabricated LTO anode delivers a sustained capacity of 202 mAh g⁻¹ in the 1.0-2.5 V range with excellent rate capability and overcomes the poor cycling stability seen in conventional defective electrodes. The feasibility of tuning the degree of structural defectiveness via quenching agents is also proven, which can open up an intriguing avenue of research to harness the intrinsic defects for improving the energy density of rechargeable batteries.

1. Introduction

Lithium-ion batteries (LIBs) are ubiquitous and so much a part of everyday life that the advent of nearly all portable electronic devices is underpinned by the breakthroughs in LIB technology.^[1] To date, graphite is extensively utilized as a commercial anode material for LIBs, owing to its low cost, high

reversibility and environmental friendliness.[2] However, the low rate capability of graphite anodes fails to meet the rising demand for high charging power, which constitutes the main bottleneck in the field of electric vehicles (EVs). According to the goal set by United States Advanced Battery Consortium, the recharge time for 80% of the pack capacity should be within 15 min to enable fast-charging EV applications.[3] Toward this end, enormous efforts have been dedicated to the development of high-rate anode materials for possible replacement of graphite. Among the potential candidates, lithium titanate (Li₄Ti₅O₁₂, LTO) is the most attractive one and has already been successfully commercialized as an anode for LIBs in public transportation.^[4] When cycling at 6C $(1C = 175 \text{ mA g}^{-1}), 90\% \text{ of its capacity}$ can be achieved within 10 min. Unfortunately, the relatively low energy density

has placed a fundamental restriction on the application domain of LTO anodes and thus resulted in a limited market share. As such, there is a renewed urgency to develop innovative strategies for boosting the reversible capacity of LTO anodes.

Ever since the first report of LTO anode in 1989,^[5] there have been continuous endeavors to understand its ion storage mechanism and to seek after a higher level of lithiation upon

Z. Su, C. Lai
School of Chemistry and Materials Science
Jiangsu Normal University
Xuzhou, Jiangsu 221116, China
Z. Su, M. Li, C. Lai, S. Zhang
Centre for Clean Environment and Energy
School of Environment and Science
Griffith University
Gold Coast Campus
Gold Coast, Queensland 4222, Australia
E-mail: s.zhang@griffith.edu.au
S. Li, M. Li, C. Dong, F. Pan
School of Advanced Materials

Peking University Shenzhen Graduate School Shenzhen 518055, China E-mail: panfeng@pkusz.edu.cn

The ORCID identification number(s) for the author(s) of this article can be found under https://doi.org/10.1002/adma.202208573.

DOI: 10.1002/adma.202208573

L. Ma

X-Ray Science Division Advanced Photon Sources Argonne National Laboratory Lemont, IL 60439, USA

T. Liu

Chemical Sciences and Engineering Division

Advanced Photon Sources Argonne National Laboratory Lemont, IL 60439, USA

T. Wu, J. Lu

College of Chemical and Biological Engineering

Zhejiang University Hangzhou 310027, China E-mail: junzoelu@zju.edu.cn

Q. Zhang, L. Gu

Beijing National Laboratory for Condensed Matter Physics

Institute of Physics

Chinese Academy of Sciences Beijing 100190, P. R. China E-mail: l.gu@iphy.ac.cn

discharge. LTO crystalizes in spinel structure, [6] with tetrahedral 8a sites occupied by Li and octahedral 16d sites occupied by randomly mixed Li and Ti ions in a ratio of 1:5. During Li intercalation, the spinel LTO undergoes a first-order phase transformation into rocksalt Li₇Ti₅O₁₂, accompanied by negligible volume change (0.2%), making LTO well known as a "zerostrain" anode that guarantees an ultralong cycle life. Moreover, LTO exhibits a flat operating potential plateau of about 1.5 V vs Li/Li+, thus circumventing the issue of lithium dendrite formation, although it also compromises the energy density of the full cells. After years of development, commercial LTO anodes could deliver over 90% of the theoretical capacity in the 1.0-2.5 V range. An intuitive way to improve the energy density is to promote excess Li intercalation into the bulk of LTO, but most of the attempts ended in vain in the past because the rocksalt Li₇Ti₅O₁₂ possesses a close-packed cation and anion lattice, which imposes severe kinetic constraints on the accommodation of extra Li ions at the interstitial sites.^[7] Although there are some observations of lithium compositions exceeding Li₇Ti₅O₁₂, it is only accessible in the subsurface regions and in the first few cycles at a normal current rate. [8] Unlocking the capacity limitations of LTO anodes still poses a great challenge, especially when the long-term cycling stability and the cost-effectiveness of treatments are simultaneously taken into account.

Defect engineering could be a key approach to conquering this difficulty.^[9] It was recently reported that oxygen-deficiency of LTO can be incurred by a strong reducing environment (H₂) during synthesis. In so doing, the overall electrochemical performance was improved due to the reduced charge-transfer resistance of the defective structure. However, these chemical

methods could only introduce defects concentrated near the surface region and at the grain boundaries where reduction reactions would occur, while bulk-related properties, such as capacity, have undergone limited changes because the surface defects could hardly activate Li ions in the interior region. Thus, it is highly desirable to develop strategies for generating and stabilizing the defects inside the bulk of the electrodes.

Herein, we manage to incorporate intrinsic defects in the bulk of nanocrystalline LTO via a straightforward heatingquenching procedure from the commercial samples. For the first time, we demonstrate the feasibility of defect engineering to alter the delithiated limit at the Li₄Ti₅O₁₂ composition, whereby the LTO anode liberates its latent reversible capacity while preserving high rate capability and cycling stability. Oxygen off-stoichiometry generated at high temperature is thus retained (Figure 1), whereas Li/Ti redistribution occurs spontaneously due to the thermodynamic driving force to resist the accumulation of V_O. This highly defective structure possesses good electronic conductivity and distinct ion storage behaviors that are absent in pristine samples. The quenched-LTO anode can reversibly extract/intercalate the native Li ions at 8a and 16d sites, which leads to a remarkable increase in capacity (up to 202 mAh g⁻¹), surpassing the theoretical and experimental values of pristine LTO by 15.4% and 30%, respectively, with excellent retention even at high rates. It is envisaged that this efficient and low-cost quenching technique can greatly expedite the development and enhance the market share of LTO-based batteries, and that the underlying mechanism will also cast new light on the design paradigm of energy-storage materials from a defect chemistry perspective.

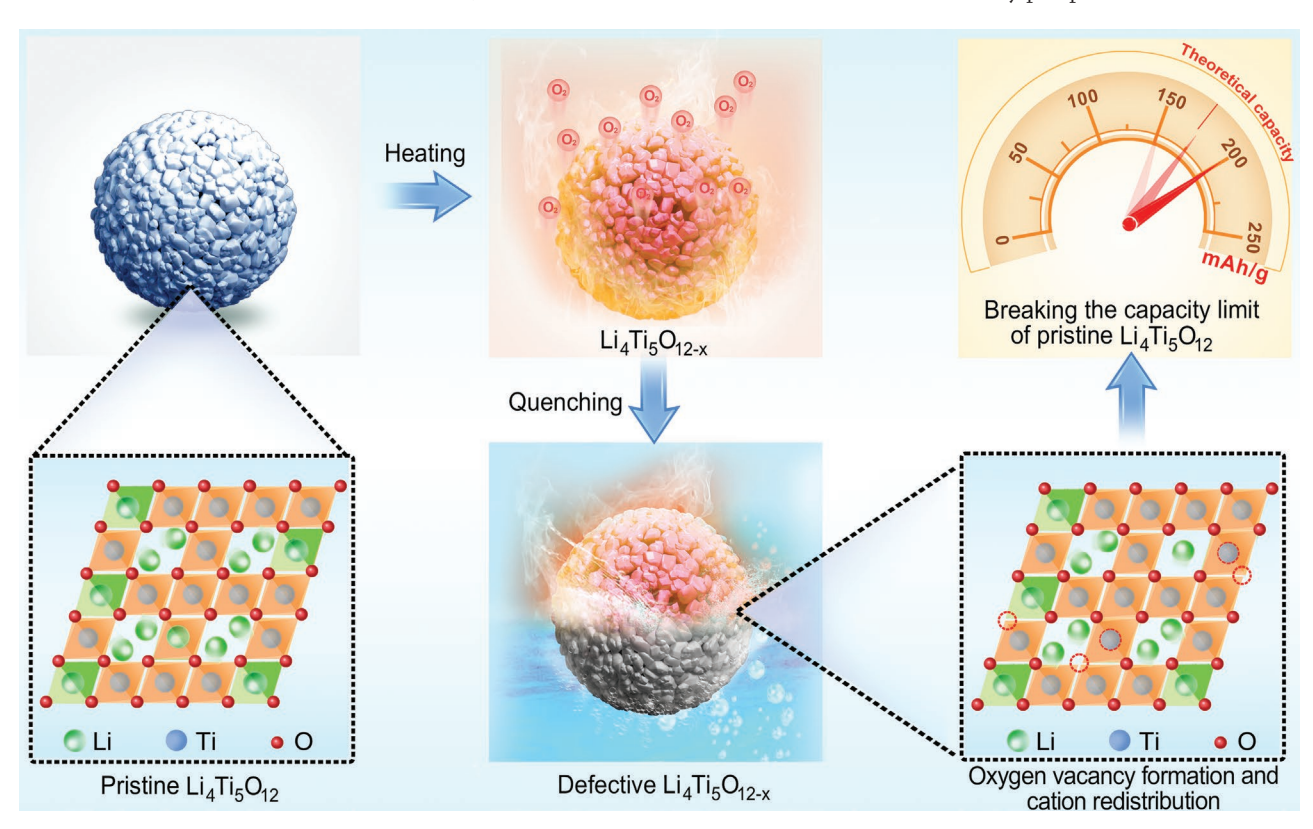


Figure 1. Conceptual representation of the structural evolution of the quenched-LTO anode during synthesis and operation.

15214095, 2023. 5, Downloaded from https://advanced.onlinelibrary.wiley.com/doi/10.1002/adma.202208573 by University Town Of Shenzhen, Wiley Online Library on [20/11/2025]. See the Terms and Conditions (https://onlinelibrary.

onditions) on Wiley Online Library for rules of use; OA articles are governed by the applicable Creative Commons

2. Results

2.1. Electrochemical Performance of the Ice-Water-Quenched LTO

The ice-water-quenched LTO (IWQ-LTO) were produced by heating a commercial LTO powder to 800 °C and then dropping it directly in ice water (detailed synthesis conditions provided in the Methods). Its performance was analyzed in a half-cell. The galvanostatic charge–discharge test of IWQ-LTO at 1C shows a specific capacity of 202 mAh g $^{-1}$ between 1.0 and 2.5 V (**Figure 2**a), which exceeds the capacity limit of traditional LTO (175 mAh g $^{-1}$) by $\approx 15.4\%$, and is 30% greater than the experimental value of the pristine sample in this study (155.4 mAh g $^{-1}$). In a test between 0 and 2.5 V at 1C, the discharge capacity of IWQ-LTO further increases to 360 mAh g $^{-1}$ (Figure S1, Supporting Information). While the discharge capacity between

0 and 1.0 V comes from the additional occupancy of Li at 8a sites near the surfaces of the rocksalt product, [8c,10] the length of the voltage plateau at $\approx\!1.5$ V is correlated with the amount of reversibly extractable Li inside the bulk phase. [4a,11] Hence, it is speculated that the increased capacity for IWQ-LTO as compared to pristine LTO at this voltage plateau is resulted from a higher degree of delithiation upon charge.

Remarkably, the rate capability and cyclability of IWQ-LTO are also outstanding. When working at 10C, IWQ-LTO can deliver a capacity of 176 mAh g⁻¹ (Figure 2b) between 1.0 and 2.5 V, which is over 40 mAh g⁻¹ higher than that of pristine LTO. For all rates tested, the capacity of this ice-water-quenched product is, to the best of our knowledge, the highest among all the LTO-based anodes (Figure 2c; Table S1, Supporting Information). After 2500 cycles at 5C, the IWQ-LTO electrode retains ≈88% of the original capacity without discernible change in the voltage profile, and has an average Coulombic efficiency of

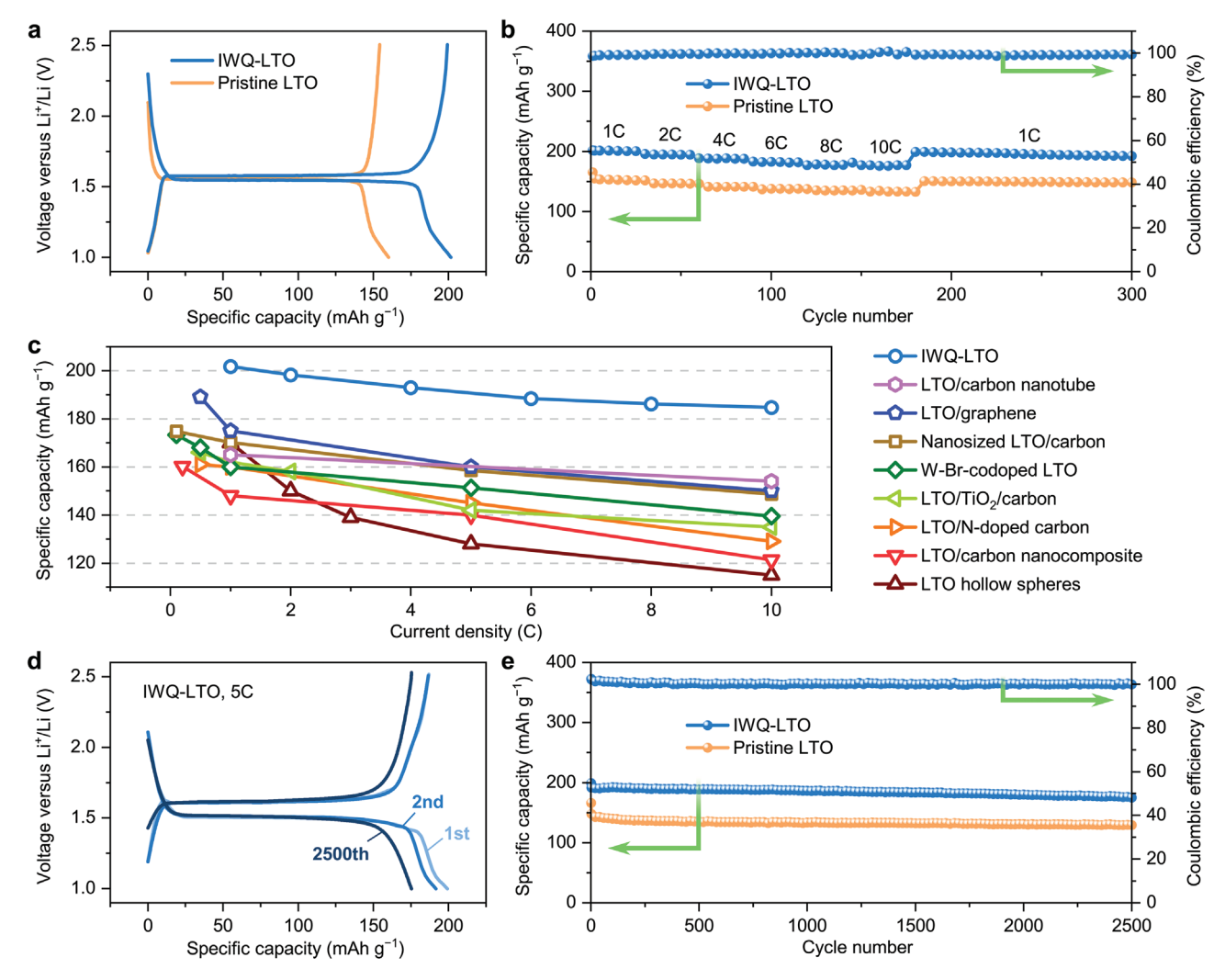


Figure 2. Electrochemical performance of IWQ-LTO electrode. a) Voltage profiles of IWQ-LTO and pristine LTO in the 1.0–2.5 V range at 1C. b) Rate performance comparison between IWQ-LTO and pristine LTO. c) Comparison of the capacity of IWQ-LTO to those of state-of-the-art LTO-based anodes as reported in the literature: LTO/carbon nanotube,^[12] LTO/graphene,^[13] nanosized LTO/carbon,^[14] W-Br-codoped LTO,^[15] LTO/TiO₂/carbon,^[16] LTO/N-doped carbon,^[17] LTO/carbon nanocomposite,^[18] and LTO hollow spheres.^[19] d) Voltage profiles of IWQ-LTO for the 1st, 2nd, and 2500th at 5C. e) Cycling performance comparison between IWQ-LTO and pristine LTO at 5C.

15214095, 2023, S, Downloaded from https://dvanced.onlinelibinary.wiley.com/doi/10.1002/adma.020208573 by University Town Of Shenzhen, Wiley Online Library on [2011/1025]. See the Terms and Conditions (https://onlinelibrary.wiley.com/terms-and-conditions) on Wiley Online Library for rules of use; OA articles are governed by the applicable Creative Commons Licensen

≈99.95% (Figure 2d,e). Scanning electron microscopy (SEM) images show negligible morphology evolution after 300 cycles (Figure S2, Supporting Information). Samples with different heating durations display similar long-term cycling stability (Figure S3, Supporting Information), suggesting that this superior performance is by no means fortuitous. In addition, the cyclic voltammetry (CV) measurements indicate a slightly less pronounced polarization for IWQ-LTO than pristine LTO (Figure S4, Supporting Information), which can be mainly attributed to the enhanced electronic conductivity in the highly defective structure given the negligible change in particle size after heating-quenching treatment (Figure S5, Supporting Information).^[20] This finding coincides with the outcomes from the analysis of electrode impedance spectra (Figure S6, Supporting Information).^[21] We have also calculated the lithium diffusion coefficient (Figure S6 and Table S2, Supporting Information), which is significantly improved in IWQ-LTO as compared with pristine LTO.

2.2. Characterization of the Ice-Water-Quenched LTO

In situ and ex situ spectroscopy techniques were used to analyze the structural evolution during the synthesis of IWQ-LTO. According to the theoretical dependence of V_O concentration on temperature, i.e., $n = N\exp(-\Delta G_V/kT)$ (N is the total number of normally occupied atom sites, ΔG_V is the Gibbs free energy for the formation of a vacancy, k is the Boltzmann constant, and T is temperature), [22] oxygen deficiency would accumulate upon heating. We employed in situ thermogravimetric analysis (TGA) to keep track of the mass change during alternating slow heating and cooling of LTO (Figure 3a). The periodic fall and rise of the TGA curve implies the release and uptake of oxygen.[23] Note that the TGA results can only afford preliminary information for the defect content, whereas X-ray absorption spectroscopy (XAS) measurements can be accurately related to the valency of metal ions. In situ X-ray absorption near-edge structure (XANES) was therefore utilized to probe the oxidation states of Ti ions at various temperatures (Figure 3b). The systematic shift of the Ti K-edge to lower energies at elevated temperatures proves the reduction of Ti4+ ions to Ti³⁺ (Figure 3c),^[24] thus adding credence to the idea that Vo are formed during heating. The average oxidation state of Ti, reaching +3.5 at 800 °C, goes back to around +3.9 upon natural cooling to room temperature (Figure 3d,e), which suggests the annihilation of V_{O} and the recovery of the structure close to pristine Li₄Ti₅O₁₂. Another justification of the depletion of lattice O ions at high temperatures comes from the in situ X-ray absorption fine structure (XAFS) measurements, which reveal the continuous decrease in amplitudes of Ti-O and Ti-Ti peaks during heating (Figure S7, Supporting Information). This trend can be rationalized by the formation of V_O, and is reversed when the sample is naturally cooled down (Figure S8, Supporting Information).^[24a]

As compared to natural cooling that permits the recombination of $V_{\rm O}$ and external oxygen in the cooling process, the quenched samples do not have enough time to be restored to their perfect crystal structure. Presumably, this highly defective structure encompassing large quantities of $V_{\rm O}$ will be stabilized

after quenching due to the limited kinetics of Ti and O ions at room temperature. The morphology of IWQ-LTO is revealed by SEM images, which indicate the formation of micro-spherical secondary particles (3-6 µm) comprising relatively loose aggregates of nanosized grains (Figure S9, Supporting Information). In the XANES spectra, a substantial discrepancy between the pristine and quenched samples is witnessed (Figure 3b). The oxidation state of Ti in IWQ-LTO is estimated to be 3.55 (Figure 3e), validating the significant off-stoichiometry. The high-resolution X-ray photoelectron spectroscopy (XPS) O 1s spectrum of IWQ-LTO (Figure 4a) can be deconvoluted into lattice O (529.8 eV), VO (531.3 eV), and adsorbed O (532.3 eV).[25] We note that the shift of the O 1s peaks between pristine LTO and IWQ-LTO is consistent with the results of oxygen-deficient TiO₂ reported in the literature.^[26] In the XPS Ti 2p spectrum (Figure 4b), a new peak emerges at 458.2 eV, indicative of Ti³⁺ ions.^[25] This result is compatible with the Raman spectra showing the blueshift of the peak at ≈140 cm⁻¹ that implies the reduction of Ti⁴⁺ (Figure S10, Supporting Information).[27] The TGA data of IWQ-LTO at 800 °C in N₂ atmosphere (Figure S11, Supporting Information) reveal a lower mass loss than pristine LTO, which is attributable to a concentration of V_O being closer to its equilibrium value at high temperature. [28] The results of XAFS (Figure S7, Supporting Information) are consistent with the above analysis, in which a less pronounced Ti-O peak in IWQ-LTO than the pristine sample is most probably linked with the removal of lattice O ions.[24a] We have tested the XPS of IWQ-LTO after exposing the sample to the air for 7 days, and the preservation of substantial oxygen deficiency is justified (Figure S12, Supporting Information), indicating considerably high stability of these defects at room temperature.

Nearly all the X-ray diffraction (XRD) peaks of the IWQ-LTO sample can be assigned to a spinel structure with a space group of Fd-3m^[29] (Figure 4c). Rietveld refinement of the XRD data has unveiled the cation rearrangement, showing that the Ti content at 16d sites is increased from 83.3 at% in pristine LTO to 88.5 at% after ice-water quenching. We note that there exist some impurity phases (IP), all of which can be indexed to an orthorhombic structure. Nevertheless, their amount is negligibly small (<5%) and can hardly influence the capacity on a large scale.

The defect enrichment is also confirmed by the high-angle annular bright-field scanning transmission electron microscopy (HAABF-STEM) images shown in Figure 4d,e. The [110] HAABF-STEM images demonstrate the preservation of Ti sublattice in a spinel structure after quenching, while the intensity profiles crossing the O columns indicate subtle differences between both samples. Variations of intensity among different O sites are clearly observed in IWQ-LTO, which drastically contrasts with the uniform pattern in the pristine material that represents an intact O sublattice. This directly supports the absence of O at specific sites in the quenched sample.^[30] Moreover, the reduction of Ti ions can be further corroborated by STEM electron energy loss spectroscopy measurements (Figure S13, Supporting Information), which reveal the rise of the O $2p \rightarrow Ti \ 3d(e_{\sigma})$ peak and the decay of the O $2p \rightarrow Ti \ 3d(t_{2\sigma})$ peak within the 530-538 eV region, a typical signature of increasing Ti³⁺ species.^[31]

15214095, 2023, 5, Downloaded from https://advanced.

onlinelibrary.wiley.com/doi/10.1002/adma.202208573 by University Town Of Shenzhen, Wiley Online Library on [20/11/2025]. See the Terms

and-conditions) on Wiley Online Library for rules of use; OA articles are governed by the applicable Creative Commons License

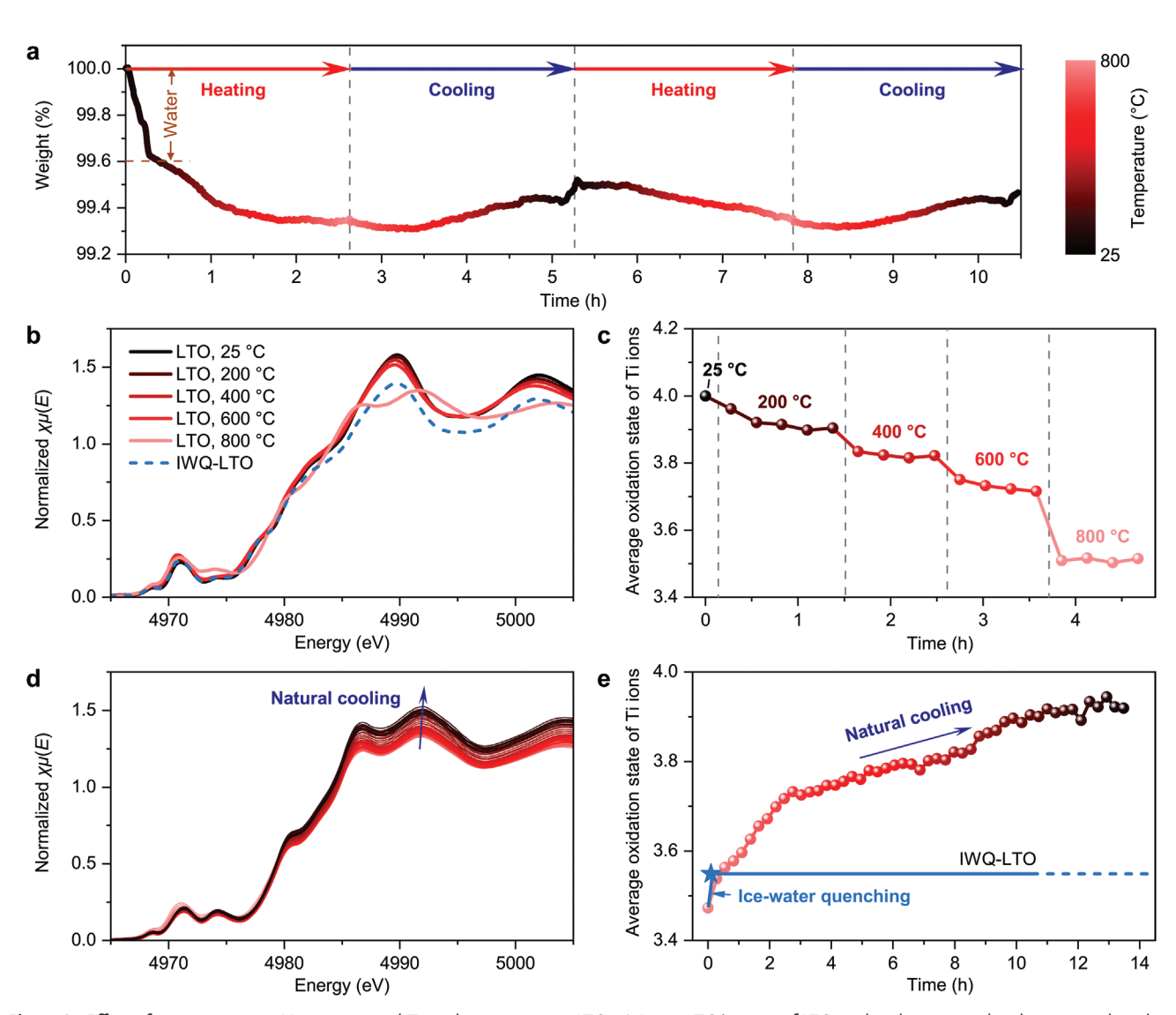


Figure 3. Effect of temperature on V_O content and Ti oxidation states in LTO. a) In situ TGA curve of LTO under alternating slow heating and cooling sequences. The intensity of red and black color of the data points and curves analogically indicates the temperatures of the samples. b) In situ XANES spectra of LTO heated to different temperatures. c) The oxidation states of Ti ions as deduced from the in situ XANES spectra of LTO at elevated temperatures. d,e) The evolution of XANES spectra of LTO during natural cooling (d) and the corresponding oxidation states of Ti (e). The XANES spectrum of LTO after ice-water quenching is also plotted in (b), and the corresponding valency of Ti is provided in (e).

A perceptible color change of LTO from white (pristine) to green (IWQ) is found, which agrees with the dramatic difference in the ultraviolet–visible (UV–vis) absorption spectra (Figure S14, Supporting Information). The existence of defect levels in the bandgap of IWQ-LTO, as inferred from the UV–vis results (Figure S15, Supporting Information), [32] is consistent with the density functional theory (DFT) calculations for the oxygen-deficient LTO structure (Figure S16, Supporting Information). Together, the spectroscopic data and observations unambiguously prove the high degree of structural defectiveness in IWQ-LTO.

2.3. Li Storage Mechanism in Quenched LTO

We propose two mechanisms, one involving V_O and the other involving Li/Ti redistribution, both of which can allow for a

capacity beyond the theoretical value of pristine LTO (Figure 5). Here, the structures of Li₄Ti₅O₁₂ and Li₇Ti₅O₁₂ are represented as $[Li_3]^{8a}[Li_1Ti_5]^{16d}[O_{12}]^{32e}$ (spinel) and $[Li_6]^{16c}[Li_1Ti_5]^{16d}[O_{12}]^{32e}$ (rocksalt), respectively. In the discharge process of Li₄Ti₅O₁₂, Li ions are inserted into one-half of the octahedral 16c sites, with the remaining half occupied by the existing Li migrating from the 8a sites. This is a two-phase transition reaction corresponding to a capacity of 3 Li per formula unit (f.u.). The oxygen-deficient $[Li_3]^{8a}[Li_1Ti_5]^{16d}[O_{12-x}]^{32e}$ yields the same amount of capacity in the first discharge process (Mechanism 1 in Figure 5). However, there are a larger number of Ti³⁺ ions in the discharged product, $[Li_6]^{16c}[Li_1Ti_5]^{16d}[O_{12-x}]^{32e}$, than the defect-free Li₇Ti₅O₁₂, owing to the extra electrons introduced by V_O. If all the Ti ions are oxidized to Ti⁴⁺ in the subsequent charge process, a total of 3+2x Li/f.u. will be deintercalated, and thereby the specific capacity in the following cycles would exceed that of pristine LTO (3 Li/f.u.). According to DFT

15214095, 2023, 5, Downloaded from https://adv.

nlinelibrary.wiley.com/doi/10.1002/adma.202208573 by University Town Of Shenzhen, Wiley Online Library on [20/11/2025]. See the Terms

-conditions) on Wiley Online Library for rules of use; OA articles are governed by the applicable Creative Commons l

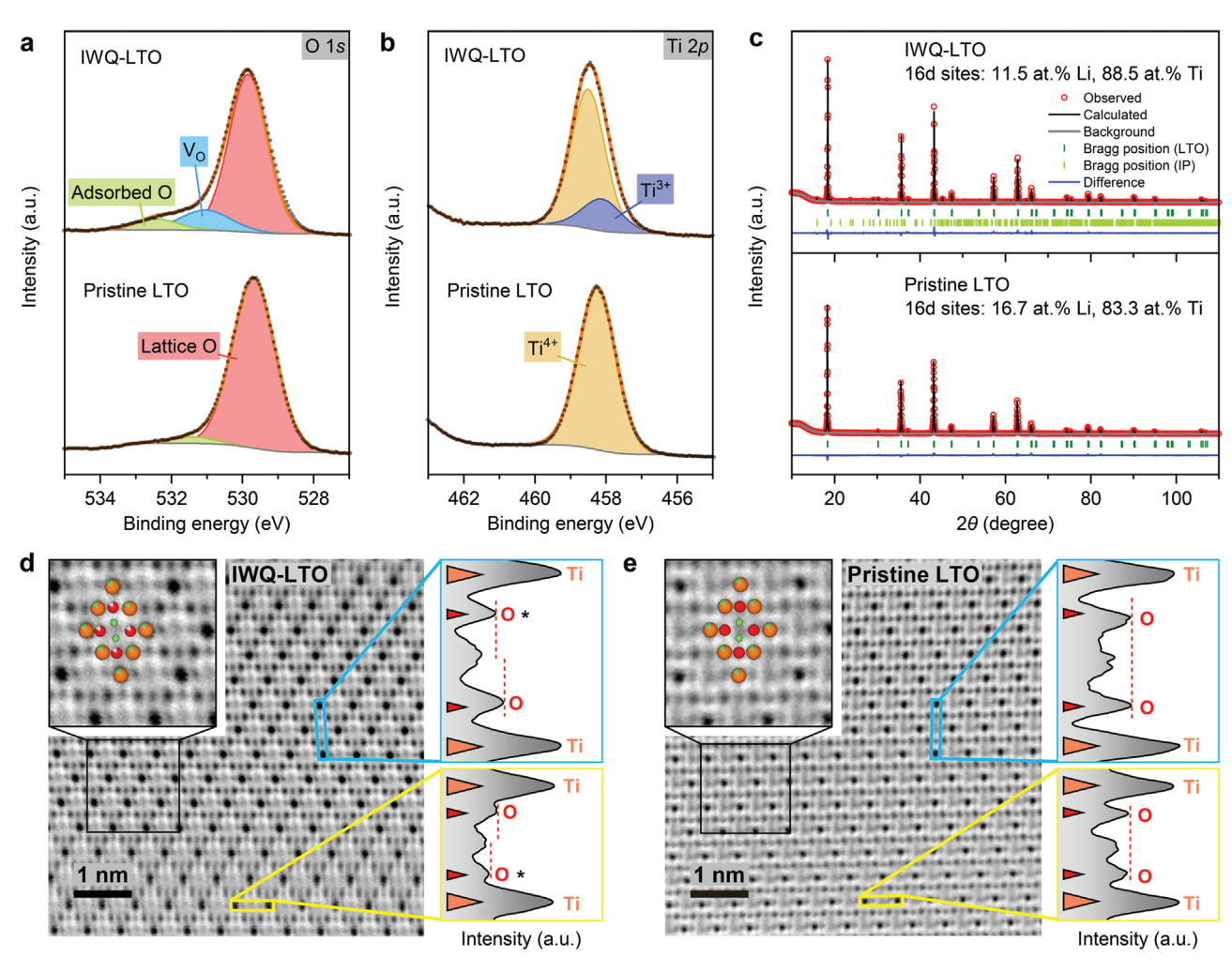


Figure 4. Characterization of IWQ-LTO and pristine LTO. a,b) XPS O 1s (a) and Ti 2p (b) spectra of IWQ-LTO (top) and pristine LTO (bottom). C) XRD patterns and Retvield refinement of IWQ-LTO (top) and pristine LTO (bottom). The Li/Ti ratios at 16d sites are 88.5 and 83.3 at% for IWQ-LTO and pristine LTO, respectively. d,e) [110] HAABF-STEM images of IWQ-LTO (d) and pristine LTO (e). The intensity profiles highlight the nonuniform distribution of O ions among the O atomic columns in IWQ-LTO, where columns marked with star symbols indicate excessive V_O. Color code: Ti, orange; O, red; Li, green.

calculations, the charged product is $[\mathrm{Li}_{3-x}]^{8a}[\mathrm{Li}_{1-x}\mathrm{Ti}_5]^{16d}[\mathrm{O}_{12-x}]^{32e}$ since it is the most energetically favorable configuration at this composition (Figures S17 and S18, Supporting Information). In this scenario, 2x Li ions per f.u. is additionally activated, and it would account for 2x/3 relative increase in the total capacity as referenced to pristine LTO. Since the V_O content is x/12, the ratio between relative capacity increase and V_O content is ((2x/3)/(x/12)) = 8. Hence, we can expect that a concentration of 1 at% V_O could contribute to 8% increase in the capacity of the anode. DFT calculations predict an average Li (de)intercalation potential of 1.56 V for a structure with about 3 at% V_O , which is slightly higher than that of the pristine LTO anode (1.45 V).

Superconcentrated $V_{\rm O}$ could facilitate atomic rearrangement so as to relieve internal stress. One viable avenue is to squeeze the vacancies out of the bulk phase and concurrently push the Li ions located at 16d sites to the 16c sites (blue dashed rectangle in Figure 5). As a result, the anion sublattice retains its perfect structure while the Li/Ti ratio on 16d sites deviates from 1:5. It is worth emphasizing that the stoichiometry of $\text{Li}_4\text{Ti}_5\text{O}_{12-x}$ and

the Ti oxidation state are supposed to be kept constant during this structural transition. Hence, the process of $V_{\rm O}$ elimination is different from the classical microscopic picture of external oxygen incorporated into the vacant site, which sees no need for the redistribution of other cations. Since Li at the 16c sites in a spinel structure is unstable, the following reaction will take place:

$$\begin{split} \left[\text{Li}_{3}\right]^{8a} \left[\text{LiTi}_{5}\right]^{16d} \left[O_{12-x}\right]^{32e} &\to \frac{3-x}{3} \left[\text{Li}_{3}\right]^{8a} \left[\frac{\text{Li}_{12-6x} \text{Ti}_{60}}{12-x}\right]^{16d} \left[O_{12}\right]^{32e} \\ &+ \frac{x}{4} \left[\text{Li}_{6}\right]^{16c} \left[\frac{\text{Li}_{12-6x} \text{Ti}_{60}}{12-x}\right]^{16d} \left[O_{12}\right]^{32e} \end{split} \tag{1}$$

with the first and second terms being the spinel and rocksalt phases, respectively. The configuration with Li/Ti redistribution has different redox reactions (Mechanism 2 in Figure 5, detailed formulation given in the Supporting Information) from that of V_O . After the first cycle, the extractable content of Li would become 3 + x per unit of $\text{Li}_4\text{Ti}_5\text{O}_{12-x}$, indicating that 1 at% of original V_O can produce 4% increase in the capacity after the

15214095, 2023, 5, Downloaded from https:

minelibrary.wiley.com/doi/10.1002/adma.20208573 by University Town Of Shenzhen, Wiley Online Library on [2011.2025]. See the Terms and Conditions (htps://onlinelibrary.wiley.com/terms-and-conditions) on Wiley Online Library for rules of use; OA articles are governed by the applicable Creative Commons.

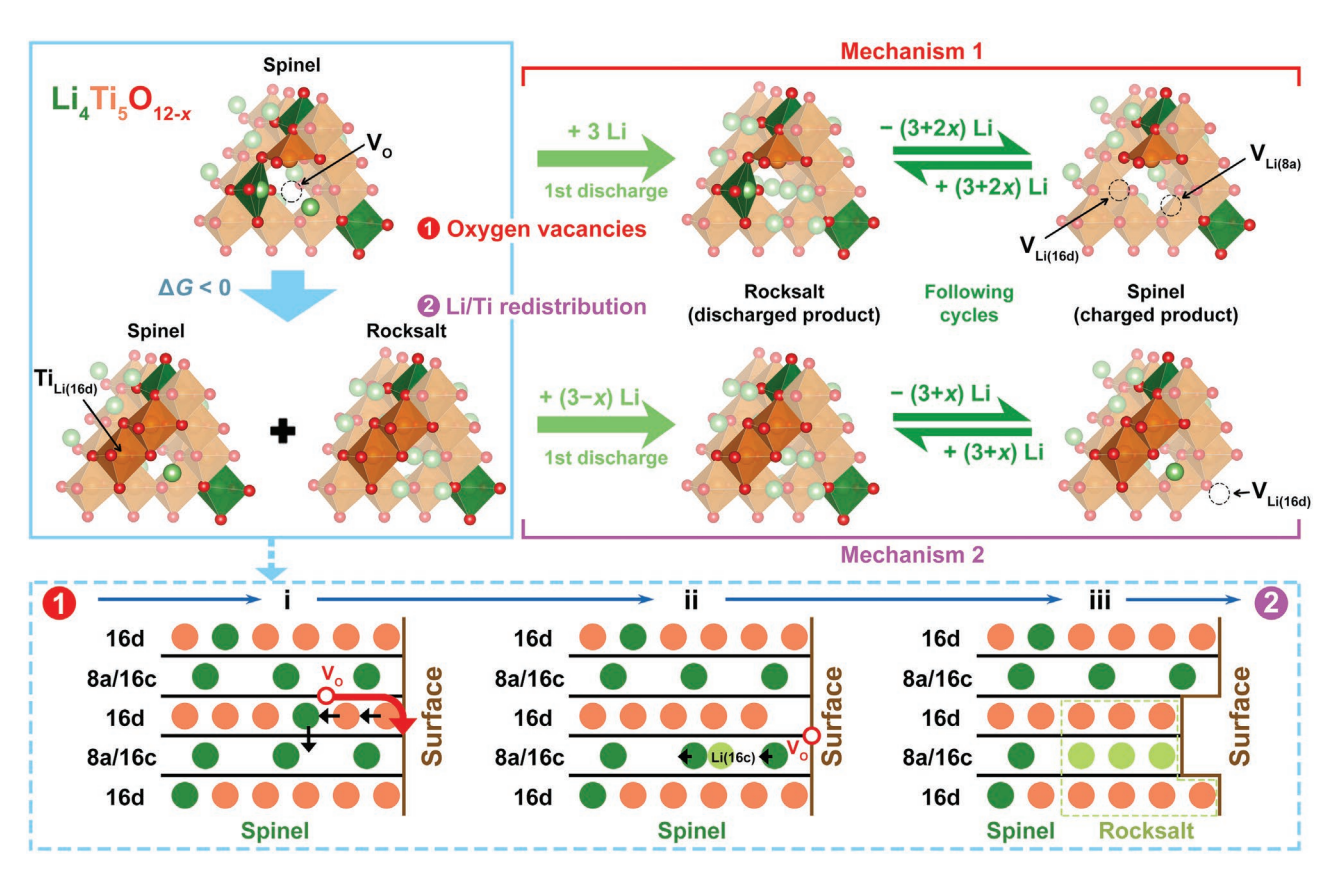


Figure 5. The influence of V_O and cation redistribution on the capacity of LTO. Li₄Ti₅O_{12-x} is taken as the initial state, which has a tendency to be transformed into a configuration with Li/Ti redistribution (blue solid rectangle). The transformation (blue dashed rectangle) involves the diffusion of V_O to the surface (i) and the synergistic displacement of cations (ii), resulting in the emergence of a small amount of rocksalt phase and the shrinkage of the oxygen sublattice (iii). In Mechanism 1, every $x \ V_O$ per f.u. of Li₄Ti₅O_{12-x} leads to an excess capacity of $2x \ \text{Li/f.u.}$ after the first discharge. In Mechanism 2, assuming that the stoichiometry of Li₄Ti₅O_{12-x} is maintained after Li/Ti redistribution, an excess capacity of $x \ \text{Li/f.u.}$ would be expected.

atomic rearrangement. A lower capacity than Mechanism 1 is therefore anticipated for Mechanism 2 with the same amount of original V_O . Nevertheless, Reaction (1) tends to be exothermic according to the DFT calculation results ($\Delta G = -1.1 \text{ eV/f.u.}$ at x = 0.57; see Figure S19 in the Supporting Information), which suggests improved thermodynamic stability after the atomic rearrangement, and consequently a high likelihood of Mechanism 2 is encountered.

It is worth mentioning that the amount of Li at 16d sites is decreased from 16.7 at% in pristine LTO to 11.5 at% in IWQ-LTO (Figure 4c). The corresponding amount of V_O leading to this rearrangement is 5.8 at% (x=0.7 in Equation (1)), which can yield up to 23% larger capacity than the theoretical value of pristine LTO. However, as the concentration of V_O and the proportion of Ti^{3+} ions cannot be unambiguously quantified from the spectroscopic measurements, we are precluded from directly assessing the individual contributions of V_O and 16d-Li/Ti ratio to the release of latent capacity. Nevertheless, we believe that both mechanisms could occur simultaneously. More importantly, a robust conclusion can still be drawn that the experimentally obtained IWQ-LTO is severely off-stoichiometric with significant participation of V_O and cation redistribution as the key factors that differ its structure from that of pristine LTO.

To further substantiate the theoretical analysis, we conducted ex situ XANES measurements to investigate oxidation states of Ti ions in the first cycle (Figure 6a-c). At the initial state, the average valency of Ti in IWQ-LTO is much lower than that of pristine LTO. After the first discharge, the discrepancy in oxidation states between both samples is reduced. Given that the valence change of Ti is linearly correlated with the amount of Li intercalation, [33] this result is indicative of less intercalated Li in IWQ-LTO than pristine LTO, which agrees well with the theoretical expectation (3 - x Li/f.u.) for the case of Li/Ti redistribution (Figure 5). Here, caution has to be exercised when considering the actual capacity of the first discharge as shown in Figure 2d, since a proportion of the capacity likely stems from surface reactions.^[34] During the subsequent charge, most of the Ti³⁺ ions are oxidized to Ti⁴⁺, resulting in fairly close average oxidation states for both IWQ-LTO and its counterpart. We note that a larger valence change of Ti is observed for IWQ-LTO at this time, meaning that the amount of deintercalated Li in IWQ-LTO exceeds pristine LTO. It can be drawn that a certain amount of native Li in the bulk of the as-prepared IWQ-LTO will be lost after the first discharge-charge cycle, which is exactly in line with the mechanistic scenario outlined above for the acquisition of additional capacity. XAFS spectra (Figure 6d,e) show the elongation of Ti-Ti bonds after the first discharge, which can be ascribed to the expansion of the lattice upon Li intercalation. After charge, the Ti-Ti bond length in IWQ-LTO shrinks to a value lower than its initial

15214095, 2023, 5, Downloaded from https://advanced.

onlinelibrary.wiley.com/doi/10.1002/adma.202208573 by University Town Of Shenzlen, Wiley Online Library on [2011/2025]. See the Terms and Conditions (https://onlinelibrary.wiley.com/terms-and-conditions) on Wiley Online Library for rules of use; OA articles are governed by the applicable Creative Commons License

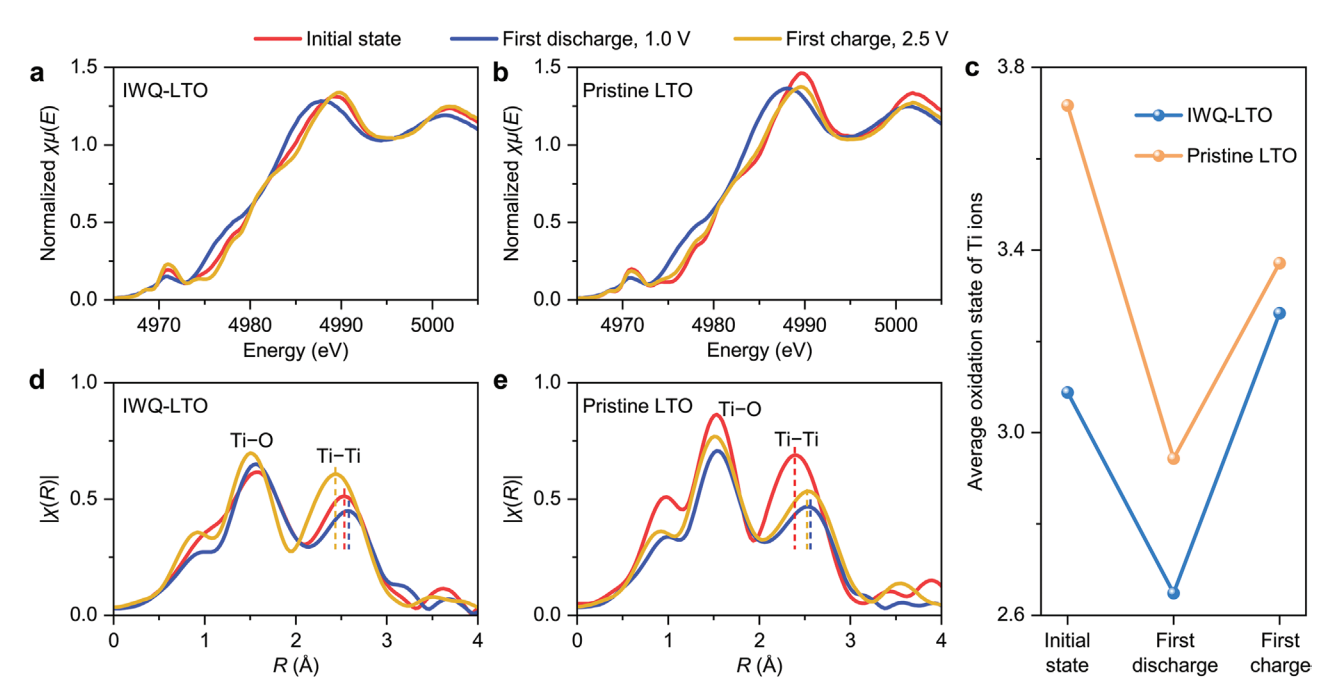


Figure 6. Li (de)intercalation in the first cycle. a–c) Ex situ XANES spectra of IWQ-LTO (a) and pristine LTO (b) at the initial, 1.0 V discharged and 2.5 V charged states, and the corresponding oxidation states of Ti ions (c). d,e) XAFS spectra of IWQ-LTO (d) and pristine LTO (e) in the first discharge–charge cycle.

value, in sharp contrast to the pristine LTO where the bond length change is essentially irreversible. This result is parallel to the trend of Ti oxidation state and implies a higher degree of delithiation in IWQ-LTO.

We have also carried out in situ XRD to examine the structural evolution of pristine LTO and IWQ-LTO during charge and discharge process. As shown in Figure S20 (Supporting Information), the peak positions of (111), (311), and (400) crystal planes in pristine LTO and IWQ-LTO undergo slight scale shifts during charge/discharge cycling. The change in lattice parameters is negligible, consistent with the zero-strain property of LTO. More importantly, comparing the in situ XRD data of pristine LTO and the IWQ-LTO, we found that there is obvious hysteresis for the (111) peak of pristine LTO during cycling, while this is not observed in IWQ-LTO. In pristine LTO, the (111) peak remains nearly unchanged in the early stage of discharge and starts to move to a higher angle afterward, but in IWQ-LTO, this peak steadily shifts to higher angle from the beginning of discharge. The overall evolution of (111) peak for IWQ-LTO shows better symmetry, indicating the excellent reversibility of Li intercalation and extraction in long-term cycling, which is consistent with the ex situ XAS results.

2.4. Effective Tuning of Defect Concentration and Electrochemical Performance

Ice water is an ideal quenching agent due to its low cost and high efficiency, which makes it suitable for industrial production of quenched LTO. Here, we show that the concentration of $V_{\rm O}$ and the Li/Ti ratio on 16d sites can be effectively tuned by the choice of quenching agent, which enables the modulation

of the electrochemical performance of the quenched LTO anodes. As a demonstration, we have replaced ice water with liquid nitrogen. It is noteworthy that although the temperature of liquid nitrogen is below that of ice water, the cooling rate of substances in liquid nitrogen is lower than in ice water due to the Leidenfrost phenomenon.^[35] The liquid-nitrogen-quenched LTO (LNQ-LTO) exhibits morphological features similar to IWQ-LTO according to the SEM images (Figure S21, Supporting Information). HAABF-STEM image supports evidence to confirm the existence of VO inside the bulk phase (Figure S22, Supporting Information). We estimate the concentration of Ti³⁺ ions via XANES, while the V_O content near the surface region can be roughly quantified by XPS measurements. As illustrated in Figure 7a,b and Figures S23 and S24 (Supporting Information), LNQ-LTO is less defective than IWQ-LTO. It appears that a lower quenching rate could lead to a lower degree of oxygen deficiency, because the recombination with external oxygen is more pronounced. XRD refinement suggests a Ti content of 87.6 at% at 16d sites in LNQ-LTO (Figure 7c), meaning that the Li/Ti redistribution is less prominent than in IWQ-LTO. The Li/Ti redistribution level in LNQ-LTO can contribute to a maximum increase of 19% in capacity with respect to pristine LTO.

A reversible capacity of 187 mAh $\rm g^{-1}$ is achieved in LNQ-LTO over the 1.0–2.5 V range at a current rate of 1C (Figure 7d). The increased capacity as compared to pristine LTO can be ascribed to the elongation of the \approx 1.5 V plateau, implying an elevated degree of delithiation upon charge, similar to the case of IWQ-LTO. An extended cycling test at 5C shows that LNQ-LTO can output 165 mAh $\rm g^{-1}$ after 300 cycles (Figure 7e), which is higher than pristine LTO, but beneath that of IWQ-LTO. The inferior electrochemical performance of LNQ-LTO in comparison to IWQ-LTO corroborates our reasoning that the excess

15214095, 2023, 5, Downloaded from https://advanced.

onlinelblary.wiley.com/doi/10.1002/adma.202208573 by University Town Of Shenzhen, Wiley Online Library on [2011/2025]. See the Terms and Conditions (thps://onlinelblary.wiley.com/terms-and-conditions) on Wiley Online Library for rules of use; OA articles are governed by the applicable Creative Commons

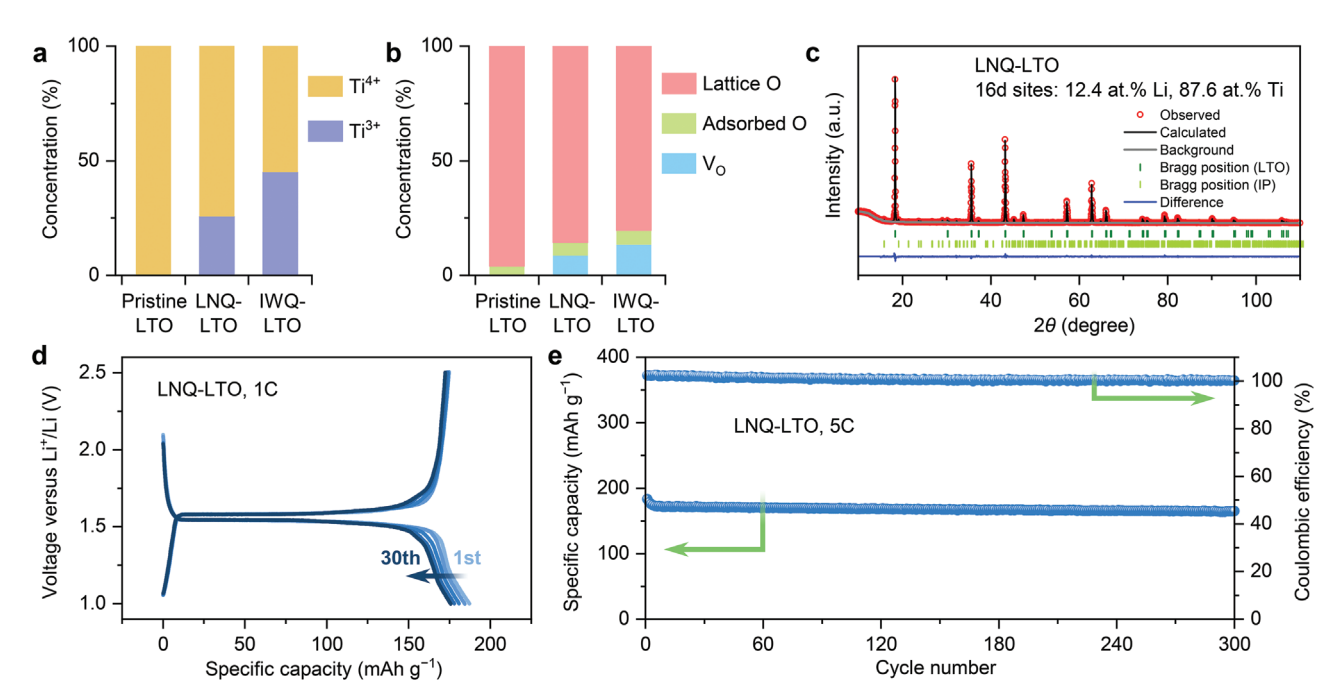


Figure 7. Characterization and electrochemical performance of LNQ-LTO. a) Concentration of Ti^{3+} as estimated from XANES. b) Concentration of V_O as estimated from XPS. c) XRD pattern and Retvield refinement of LNQ-LTO. d) Voltage profile of LNQ-LTO between 1.0 and 2.5 V at 1C. e) Cycling performance of IWQ-LTO at 5C for 300 cycles.

specific capacity of the quenched product arises from $V_{\rm O}$ and Li/Ti redistribution, and hence is proportional to the degree of structural defectiveness. Furthermore, based on the above findings, it is feasible to fine-tune the structural defectiveness via the adjustment of quenching conditions, including the quenching agent and the initial heating temperature (Figure 3c), which offers hope for the optimization of such quasi-equilibrium defective structures for the design of highly performing LIB electrodes.

3. Conclusions

We have demonstrated the opportunities offered by intrinsic defects to activate Li ions that are conventionally not extractable in an electrode material. As exemplified by the LTO anode, highly defective structures with abundant Vo and cation redistribution can be realized via a heating-quenching treatment, a technique that can be directly applied to current commercial electrodes. In situ and ex situ spectroscopy techniques have confirmed the oxygen off-stoichiometry with which native Li ions in LTO can readily be extracted during delithiation owing to the introduction of excess electrons. By virtue of the stabilized defects after ice-water quenching, a sustained reversible capacity of 202 mAh g-1 is achieved between 1.0 and 2.5 V, reaching 115.4% (130%) of the theoretical (experimental) capacity of pristine LTO. A specific capacity of 176 mAh g⁻¹ is retained even at 10C. The tunable defect concentration depending on the choice of quenching agent allows us to further optimize the electrochemical performance. We believe that our discovery can be generalized to other materials systems, and the quenching treatment can be implemented as

a cost-effective strategy for intrinsic defect engineering, which can be leveraged in an industrial context to promote the energy density of existing electrodes for use in EVs.

4. Experimental Section

Material Preparations: The IWQ-LTO sample was prepared from commercial LTO powder (Tianjin Jiewei). Pristine LTO (5 g) was first sonicated in 3 mol L $^{-1}$ NaCl solution for several hours. After centrifugation and removing the supernatant solution, the sample was dried at 60 °C for 3 h, heated at 800 °C for 0.5 h in the muffle furnace, and then thrown into ice water immediately. At last, the quenched sample was dried at 80 °C for 6 h. LNQ-LTO was prepared within the same method and different quenching agent.

Material Characterization: The X-ray absorption near-edge structure (XANES) spectra at Ti K-edge was collected in transmission mode and XANES data reduction and analysis were processed by Athena software. Pristine $Li_4Ti_5O_{12}$ at room temperature was taken as the reference material for the calibration curve. The X-ray photoelectron spectroscopy (XPS) spectra were conducted on a multifunctional imaging electron spectrometer (Thermo ESCALAB 250XI, Monochromatized Al Klpharesource). Scanning electron microscopy (SEM, SU8020) and highresolution transmission electron microscopy (HRTEM, Tecnai G20) were conducted to characterize the morphology and structure of the obtained LTO. The atomic structure was characterized using an ARM-200CF (JEOL, Tokyo, Japan) transmission electron microscopy (TEM) operated at 200 keV and equipped with double spherical aberration (Cs) correctors. The angular bright-field (ABF) images were acquired with a collection angle of 12-24 mrad. The spot size was chosen to be 8C to avoid electron bean irradiation. The fine structure of the electron energy loss spectroscopy (EELS) spectrum was obtained with an energy resolution about 0.5 eV at 200 keV. XRD pattern was collected on a Cu-K α radiation (λ = 1.5405 Å) and the diffraction pattern with Rietveld refinement was performed by the RIETAN-2000 program. Raman spectra were examined on a Renishaw system 100 Raman fiber

15214095, 2023, 5, Downloaded from https://dwarced.onlinebbary.wikey.com/ois/10.1002/adma.02208573 by University Town Of Shenzhen, Wiley Online Library on [2011/2025]. See the Terms and Conditions (https://onlinebbary.wiley.com/terms-and-conditions) on Wiley Online Library for rules of use; OA articles are governed by the applicable Centifier Commons.

spectrometer and UV–vis diffusion reflectance spectra were collected on a Thermo Nicolet Evolution 500 UV–vis spectrophotometer. Thermogravimetric analysis (TGA) measurement was performed on a Rigaku Thermoflex PTC-10A thermal analyzer with a heating rate of 5 $^{\circ}\text{C}$ min $^{-1}$ in air or N $_2$ atmosphere.

Electrochemical Measurements: The galvanostatic charge–discharge cycling was studied on a LAND-CT2001A battery tester at different rates (1C = 175 mA g $^{-1}$) within the voltage range of 1–2.5 V. The electrolyte was 1 m LiPF $_6$ in a 1:1:1 (w/w) mixture solution of ethyl carbonate (EC), ethyl methyl carbonate (EMC) and dimethyl carbonate (DMC). Working electrodes (around 1 mg cm $^{-2}$ in loading) were prepared by mixed LTO, carbon black and polyvinylidene fluoride (PVDF) in a weight ratio of 7:2:1, with N-methyl pyrrolidinone as the dispersant, on a copper foil and dried at 60 °C for 24 h. CV and electrochemical impedance spectroscopy (EIS, frequency 100 kHz to 10 MHz) were carried on a CHI660D electrochemical workstation.

DFT Calculations: DFT calculations were performed using Vienna Ab initio Simulation Package (VASP). [36] The electron–core interactions were treated in the projector augmented wave method [37] with a cutoff energy of 520 eV. The Perdew–Burke–Ernzerhof exchange-correlation functional [38] was employed with Hubbard U corrections (PBE+U) to take account of the on-site Coulomb interaction. [39] The value of 4.2 eV for the U parameter of Ti ion was adopted from previous studies. [40] The k-point sampling density of at least 1000/(the number of atoms per cell) within the Monkhost–Pack scheme [41] was found sufficient for energy convergence.

Supporting Information

Supporting Information is available from the Wiley Online Library or from the author.

Acknowledgements

Z.S. and S.L. contributed equally to this work. The authors are grateful for the financial support from the Australia Research Council Discovery Projects DP210103266 and DP180102003, the National Key R&D Program of China (2016YFB0700600 and 2020YFB0704500), the Chemistry and Chemical Engineering Guangdong Laboratory (Grant no.1922018), the Shenzhen Science and Technology Research Grant (no. JCYJ20200109140416788), and Soft Science Research Project of Guangdong Province (no. 2017B030301013).

Conflict of Interest

The authors declare no conflict of interest.

Data Availability Statement

The data that support the findings of this study are available from the corresponding author upon reasonable request.

Keywords

intrinsic defects, lithium titanate anodes, quenching, reversible Li extraction

Received: September 18, 2022 Revised: October 31, 2022 Published online: December 23, 2022

- [1] a) M. Li, J. Lu, Z. Chen, K. Amine, Adv. Mater. 2018, 30, 1800561;
 b) J. Lu, Z. Chen, Z. Ma, F. Pan, L. A. Curtiss, K. Amine, Nat. Nanotechnol. 2016, 11, 1031;
 c) M. Armand, J.-M. Tarascon, Nature 2008, 451, 652.
- [2] a) C. Martin, Nat. Nanotechnol. 2014, 9, 327; b) J. Xu, Y. Dou, Z. Wei,
 J. Ma, Y. Deng, Y. Li, H. Liu, S. Dou, Adv. Sci. 2017, 4, 1700146.
- [3] Y. Liu, Y. Zhu, Y. Cui, Nat. Energy 2019, 4, 540.
- [4] a) H. C. Chiu, X. Lu, J. Zhou, L. Gu, J. Reid, R. Gauvin, K. Zaghib, G. P. Demopoulos, Adv. Energy Mater. 2017, 7, 1601825; b) G. L. Zhu, C. Z. Zhao, J. Q. Huang, C. He, J. Zhang, S. Chen, L. Xu, H. Yuan, Q. Zhang, Small 2019, 15, 1805389; c) M. Odziomek, F. Chaput, A. Rutkowska, K. Świerczek, D. Olszewska, M. Sitarz, F. Lerouge, S. Parola, Nat. Commun. 2017, 8, 15636; d) W. Zhang, D.-H. Seo, T. Chen, L. Wu, M. Topsakal, Y. Zhu, D. Lu, G. Ceder, F. Wang, Science 2020, 367, 1030; e) J. Lu, Z. Chen, F. Pan, Y. Cui, K. Amine, Electrochem. Energy Rev. 2018, 1, 35.
- [5] K. Colbow, J. Dahn, R. Haering, J. Power Sources 1989, 26, 397.
- [6] L. Aldon, P. Kubiak, M. Womes, J. Jumas, J. Olivier-Fourcade, J. Tirado, J. Corredor, C. Pérez Vicente, Chem. Mater. 2004, 16, 5721.
- [7] a) B. Zhao, R. Ran, M. Liu, Z. Shao, *Mater Sci Eng. R.* 2015, 98, 1;
 b) H. Kim, W. Choi, J. Yoon, J. H. Um, W. Lee, J. Kim, J. Cabana, W.-S. Yoon, *Chem. Rev.* 2020, 120, 6934;
 c) T.-F. Yi, T.-T. Wei, Y. Li, Y.-B. He, Z.-B. Wang, *Energy Storage Mater.* 2020, 26, 165.
- [8] a) H. Ge, N. Li, D. Li, C. Dai, D. Wang, Electrochem. Commun. 2008, 10, 719; b) W. Borghols, M. Wagemaker, U. Lafont, E. Kelder, F. Mulder, J. Am. Chem. Soc. 2009, 131, 17786; c) S. Ganapathy, M. Wagemaker, ACS Nano 2012, 6, 8702; d) M. Wagemaker, F. M. Mulder, Acc. Chem. Res. 2013, 46, 1206; e) Y. He, A. Muhetaer, J. Li, F. Wang, C. Liu, Q. Li, D. Xu, Adv. Energy Mater. 2017, 7, 1700950.
- [9] a) Z. Yang, L. Zhu, C. Lv, R. Zhang, H. Wang, J. Wang, Q. Zhang, Mater. Chem. Front. 2021, 5, 5880; b) J. Maier, J. Electrochem. Soc. 2015; c) R. N. Nasara, P.-c. Tsai, S.-k. Lin, Adv. Mater. Interfaces 2017, 4, 1700329; d) C. Dong, W. Dong, X. Lin, Y. Zhao, R. Li, F. Huang, EnergyChem 2020, 2, 100045; e) J. Zhu, J. Chen, H. Xu, S. Sun, Y. Xu, M. Zhou, X. Gao, Z. Sun, ACS Appl. Mater. Interfaces 2019, 11, 17384.
- [10] H. Liu, Z. Zhu, J. Huang, X. He, Y. Chen, R. Zhang, R. Lin, Y. Li, S. Yu, X. Xing, Q. Yan, X. Li, M. J. Frost, K. An, J. Feng, R. Kostecki, H. Xin, S. P. Ong, P. Liu, ACS Mater. Lett. 2019, 1, 96.
- [11] Z. Zhong, C. Ouyang, S. Shi, M. Lei, ChemPhysChem 2008, 9, 2104.
- [12] J. Liu, K. Song, P. A. van Aken, J. Maier, Y. Yu, Nano Lett. 2014, 14, 2597.
- [13] J. Kim, K. E. Lee, K. H. Kim, S. Wi, S. Lee, S. Nam, C. Kim, S. O. Kim, B. Park, *Carbon* 2017, 114, 275.
- [14] L. Shen, X. Zhang, E. Uchaker, C. Yuan, G. Cao, Adv. Energy Mater. 2012, 2, 691.
- [15] Q. Zhang, H. Lu, H. Zhong, X. Yan, C. Ouyang, L. Zhang, J. Mater. Chem. A 2015, 3, 13706.
- [16] M. M. Rahman, J. Z. Wang, M. F. Hassan, D. Wexler, H. K. Liu, Adv. Energy Mater. 2011, 1, 212.
- [17] L. Zhao, Y. S. Hu, H. Li, Z. Wang, L. Chen, Adv. Mater. 2011, 23, 1385
- [18] C. Wang, S. Wang, Y.-B. He, L. Tang, C. Han, C. Yang, M. Wagemaker, B. Li, Q.-H. Yang, J.-K. Kim, Chem. Mater. 2015, 27, 5647
- [19] L. Yu, H. B. Wu, X. W. Lou, Adv. Mater. 2013, 25, 2296.
- [20] E. H. M. Salhabi, J. Zhao, J. Wang, M. Yang, B. Wang, D. Wang, Angew. Chem., Int. Ed. 2019, 58, 9078.
- [21] C. Yuan, L. Zhang, S. Zhu, H. Cao, J. Lin, L. Hou, Nanotechnology 2015, 26, 145401.
- [22] L. E. Smart, E. A. Moore, Solid State Chemistry: An Introduction, CRC Press, Boca Raton, FL, USA 2016.
- [23] a) X. Pan, M.-Q. Yang, X. Fu, N. Zhang, Y.-J. Xu, Nanoscale 2013, 5, 3601; b) S. Ghosh, G. G. Khan, K. Mandal, A. Samanta, P. Nambissan, J. Phys. Chem. C 2013, 117, 8458.



www.advancedsciencenews.com



www.advmat.de

15214095, 2023, 5, Downloaded from https://advanced.onlinelibrary.wiley.com/doi/10.1002/adma.202208573 by University Town Of Shenzhen,

Wiley Online Library on [20/11/2025]. See the Term:

and-conditions) on Wiley Online Library for rules of use; OA articles are governed by the applicable Creative Commons

- [24] a) A. Thomas, W. Flavell, A. Mallick, A. Kumarasinghe, D. Tsoutsou, N. Khan, C. Chatwin, S. Rayner, G. Smith, R. Stockbauer, Phys. Rev. B 2007, 75, 035105; b) Q. Wu, Q. Zheng, R. van de Krol, J. Phys. Chem. C 2012, 116, 7219.
- [25] G. Ou, Y. Xu, B. Wen, R. Lin, B. Ge, Y. Tang, Y. Liang, C. Yang, K. Huang, D. Zu, Nat. Commun. 2018, 9, 1302.
- [26] a) M. Xing, J. Zhang, F. Chen, B. Tian, Chem. Commun. 2011, 47, 4947; b) S. H. Chen, Y. Xiao, Y. H. Wang, Z. F. Hu, H. Zhao, W. Xie, Nanomaterials 2018, 8, 553.
- [27] C. Xu, P. Zhang, L. Yan, J. Raman Spectrosc. 2001, 32, 862.
- [28] C. Zhen, L. Wang, L. Liu, G. Liu, G. Q. Lu, H.-M. Cheng, Chem. Commun. 2013, 49, 6191.
- [29] W. Fang, P. Zuo, Y. Ma, X. Cheng, L. Liao, G. Yin, Electrochim. Acta 2013, 94, 294.
- [30] D. A. Muller, N. Nakagawa, A. Ohtomo, J. L. Grazul, H. Y. Hwang, Nature 2004, 430, 657.
- [31] E. Stoyanov, F. Langenhorst, G. Steinle-Neumann, Am. Mineral. 2007, 92, 577.

- [32] a) X. Chen, L. Liu, F. Huang, Chem. Soc. Rev. 2015, 44, 1861;
 b) X. Chen, L. Liu, Y. Y. Peter, S. S. Mao, Science 2011, 331, 746.
- [33] Y. Peng-Fei, C. Zhong-Hui, M. Jian-Wei, G. Xiang-Xin, Chin. Phys. Lett. 2013, 30, 036102.
- [34] a) H. Lu, J. Hagberg, G. Lindbergh, A. Cornell, Nano Energy 2017, 39, 140; b) Z. Yao, H. Yin, L. Zhou, G. Pan, Y. Wang, X. Xia, J. Wu, X. Wang, J. Tu, Small 2019, 15, 1905296.
- [35] B. Jehl, R. Bauer, A. Dörge, R. Rick, J. Microsc. 1981, 123, 307.
- [36] a) G. Kresse, J. Furthmüller, Comp. Mater. Sci. 1996, 6, 15;
 b) G. Kresse, J. Furthmüller, Phys. Rev. B 1996, 54, 11169.
- [37] G. Kresse, D. Joubert, Phys. Rev. B 1999, 59, 1758.
- [38] J. P. Perdew, M. Ernzerhof, K. Burke, J. Chem. Phys. 1996, 105, 9982
- [39] S. Dudarev, G. Botton, S. Savrasov, C. Humphreys, A. Sutton, Phys. Rev. B 1998, 57, 1505.
- [40] B. J. Morgan, G. W. Watson, Surf. Sci. 2007, 601, 5034.
- [41] H. J. Monkhorst, J. D. Pack, Phys. Rev. B 1976, 13, 5188.